Spectral Methods for Modeling Supersonic Chemically Reacting Flowfields

J. Philip Drummond,* M. Yousuff Hussaini,† and Thomas A. Zang*
NASA Langley Research Center, Hampton, Virginia

A numerical algorithm has been developed for solving the equations describing chemically reacting supersonic flows. The algorithm employs a two-stage Runge-Kutta method for integrating the equations in time and a Chebyshev spectral method for integrating the equations in space. The accuracy and efficiency of the technique have been assessed by comparison with an existing implicit finite-difference procedure for modeling chemically reacting flows. The comparison showed that the new procedure yielded equivalent accuracy on much coarser grids as compared to the finite-difference procedure, with significant gains in computational efficiency.

Nomenclature

A = cross-sectional area, constant in Arrhenius law
a,b = constants in specific heat equations
C = concentration of species
c = speed of sound
c_p = specific heat at constant pressure
E = activation energy
e_0 = total internal energy
F = flux vector
$\hat{F}_n, \hat{F}_n^{(1)}$ = expansion coefficients in Chebyshev series
f = mass fraction
H = source vector
h_0 = total enthalpy
H_T^0 = reference enthalpy at standard conditions
I = identity matrix
K = equilibrium constant
k_b = reverse-reaction rate
k_f = forward-reaction rate
M = molecular weight
N = number of nodes minus 1
N_R = number of reactions
N_s = number of species
p = static pressure
p_0 = total pressure
R = steady-state residual
R^0 = universal gas constant
T_0 = total temperature
T = static temperature
T_n = Chebyshev polynomial
t = time
Δt = time step
$\dot{w}$ = species production rate
U = dependent variable vector
u = velocity
x = spatial variable
Δx = spatial step size
γ = stoichiometric coefficient, ratio of specific heats
λ = eigenvalue
ρ = density
ϕ = equivalence ratio

Subscripts

c = based on chemistry
f = based on fluids
i,j = species indices
R = reactions, reference value
s = species
sp = evaluated spectrally

Superscript

$\bar{(\ )}$ = mass-weighted value

Presented as Paper 85-0302 at the AIAA 23rd Aerospace Sciences Meeting, Reno, NV, Jan. 14-17, 1985; received Feb. 15, 1985; revision received Jan. 27, 1986.

*Aerospace Engineer, Computational Methods Branch, High-Speed Aerodynamics Division. Senior Member AIAA.

†Senior Scientist, Institute for Computer Applications in Science and Engineering. Associate Fellow AIAA.

Introduction

RESEARCH to develop ramjet and supersonic combustion ramjet (scramjet) propulsion systems has been underway at the NASA Langley Research Center for a number of years. A critical element in the design of scramjets and ramjets is the detailed understanding of the complex flowfield present in the engine over a range of operating conditions. Numerical modeling of various regions of the engine flowfield has proven to be a valuable tool for gaining insight into the nature of these flows. In recent years, computer programs have been developed to model the chemically reacting flowfields in ramjet and scramjet systems.[1-3] These programs have employed both explicit and implicit finite-difference procedures to solve the equations governing the flowfield in the engine combustors. The calculations have often required long computer runs to reach desired steady-state conditions and have been quite costly, owing to stiffness introduced in the equations by the finite-rate chemical kinetics that is required for accurate modeling. Also, computer resource limitations have sometimes reduced the degree of spatial resolution that could be achieved in the calculations. These factors have led to the desire for more efficient and more highly accurate algorithms for solving chemically reacting combustor flows.

The system of partial differential equations describing chemically reacting flows [see Eq. (4)] is stiff because of the highly disparate time scales that exist among the equations. Certain chemical reactions in an overall combustor kinetics system can take place on an extremely short time scale of the order of 10^{-12} s, whereas the fluids dynamics may require 10^{-3}–10 s for a typical case to reach steady-state conditions.

There are, of course, several intermediate scales lying between these two extremes. Mathematically, stiffness is often defined by examining the eigenvalues of the Jacobian of the governing equation system and noting that the ratio of the real part of the largest eigenvalue to the real part of the smallest eigenvalue is a large number. The former physical definition is perhaps the more useful test of stiffness; it is felt directly in the numerical integration of stiff systems through the proper required choice of the integration time step. We will deal with this requirement now and then follow with a discussion concerning integration of the spatial part of the problem.

Stiffness in the system of equations governing chemically reacting flows typically arises from the source terms in the equations describing the production and loss of the chemical species that are present. Large values for these source terms produce rapid changes in the dependent variables being sought and result in the very short time scales discussed in the previous paragraph. To deal with this constraint, several authors, including Bussing and Murman,[4] Stalnaker et al.,[5] and Smoot, et al.[6] recognized that the stiff source terms in the system of equations governing chemically reacting flow should be evaluated implicitly. Therefore, for our problem, algorithms should be developed with the source terms written implicitly at the new time level in the integration step. Other terms in the governing equations that do not lead to stiffness can still be evaluated explicitly.[4-6]

Perhaps the best-known algorithms for solving stiff systems of ordinary differential equations are those developed by Gear.[7] These schemes employ Adams' methods of variable order with explicit formulas used to solve nonstiff equations in the system and implicit formulas used to solve the stiff equations. Hindmarsh[8] generalized the Gear algorithms and developed a variant to allow for a variable integration step size.[9] Another class of algorithms for effectively solving stiff ordinary differential equations is the exponential-fitted schemes, described in the works of Liniger and Willoughby[10] and of Pratt.[11] These methods fit the solution at two or more integration points with an exponential interpolant rather than the polynomial interpolants used in the Gear schemes. The exponential-fitted schemes more naturally follow the exponential behavior of solutions to chemical kinetics problems. Additionally, for decaying solutions, this class of algorithms has an infinite stability radius for both the implicit and explicit variants.[11] A good deal more work has been carried out to develop efficient and accurate algorithms for solving stiff systems of ordinary differential equations (ODE's) resulting from chemical kinetics problems. We will not continue our survey here, but, rather, we will refer readers to two interesting papers, the first by Bui, et al.[12] and the second by Radhakrishnan,[13] that further discuss the area of stiff ODE solvers.

Next we deal with the computation of spatial derivatives in the governing equations. The importance of accurately modeling spatial derivatives cannot be overemphasized. Chemical reaction does not take place until fuel and oxidant are brought together and macroscopically mixed by convective transport and then mixed down to the microscopic (molecular) level by diffusive processes. To model these processes, spatial derivatives must be accurately computed. Because of computer storage limitations, higher-order numerical methods were indicated. Higher-order finite-difference schemes offered one option for computing the spatial derivatives. Another option was apparent from earlier work of Hussaini and Zang to develop methods for highly accurate solutions of the Euler equations. Here Hussaini et al.[14,15] used a spectral collocation method to compute the required spatial derivatives in the governing equations. With this approach, several problems governed by the Euler equations were successfully solved and accurate solutions were obtained on relatively coarse grids as compared to finite-difference solutions of the same problems. Spectral methods are based on the representation of the solution to a problem f by a finite series of global functions X of the form

$$f(x) = \sum_{n=0}^{N} \hat{a}_n X_n(x) \tag{1}$$

where the $\hat{a}_n$ are the expansion coefficients of the series.[16] The X_n should be a complete orthogonal set. Spatial derivatives of f are then approximated by taking derivatives of the corresponding series of Eq. (1). If properly applied, the high-order approximation of Eq. (1) yields a very accurate numerical representation for derivatives of f. Spectral methods should therefore satisfy our requirements for approximating spatial derivatives in the equations governing a chemically reacting flowfield.

This paper discusses the development of a numerical algorithm for solving the equations governing a chemically reacting flow. The algorithm employs a two-stage, partial implicit Runge-Kutta scheme for integrating the equations in time and a Chebyshev spectral collocation method for computing spatial derivatives in the equations. A computer program has been written to apply this algorithm for the solution of a reacting flow problem. The code is currently limited to quasi-one-dimensional inviscid flows with hydrogen-air reaction, which is appropriate for development and evaluation of the algorithm. There appear to be no restrictions prohibiting extension of the algorithm to three-dimensional viscous flows. Chemical reaction is represented in the program with a finite-rate chemistry model, and a real-gas thermodynamic model is employed.

Analysis

Governing Equations

The quasi-one-dimensional Euler equations in conservation law form with multiple species undergoing chemical reaction are[17]

$$\frac{\partial U}{\partial t} + \frac{\partial F}{\partial x} + H = 0 \tag{2}$$

where

$$U = \{\rho A,\ \rho u A,\ \rho e_0 A,\ \rho f_i A\}^T \tag{3}$$

$$F = \{\rho u A,\ \rho u^2 A + pA,\ \rho u h_0 A,\ \rho u f_i A\}^T \tag{4}$$

$$H = \left\{0,\ -p\frac{dA(x)}{dx},\ 0,\ -\dot{w}_i A\right\}^T \tag{5}$$

$$h_0 = \int_{T_R}^{T} \bar{c}_p dT + \frac{u^2}{2} + \sum_{j=1}^{N_s} (H_T^0)_j f_j \tag{6}$$

$$e_0 = h_0 - (R^0/\bar{M})T \tag{7}$$

If there are N_s chemical species, then, $i = 1,2,\ldots, N_s - 1$, and $N_s - 1$ equations must be solved for the species f_i. The final species mass fraction f_{N_s} can then be found by conservation of mass, since

$$\sum_{i=1}^{N_s} f_i = 1$$

Chemistry Model

The chemical reaction of hydrogen and oxygen is modeled in this work with the global finite-rate hydrogen-air chemistry model of Rogers and Chinitz.[18] This model adequately represents the chemical reaction taking place in the problems to be considered, and it also produces an extremely large disparity in the time scales present in the problems.

This phenomenon allows the ability of the numerical algorithm to deal with resulting stiffness to be demonstrated.

The Rogers-Chinitz model assumes that the overall reaction of hydrogen and oxygen takes place through two reactions, the first resulting in the formation of a hydroxyl radical and the second combining the hydroxyl radical with hydrogen to form water. The reactions are given by

$$H_2 + O_2 \underset{k_{b1}}{\overset{k_{f1}}{\rightleftharpoons}} 2OH \tag{8}$$

$$2OH + H_2 \underset{k_{b2}}{\overset{k_{f2}}{\rightleftharpoons}} 2H_2O \tag{9}$$

where the k_f values are the forward-reaction rates and the k_b values are the reverse-reaction rates. The reverse rates can be found, given the forward rate and the equilibrium constant K for each reaction, as

$$k_b = k_f / K \tag{10}$$

The forward-reaction rates are computed from the Arrhenius law,

$$k_{f_i} = A_i T^{N_i} e^{-E_i/R^0 T} \tag{11}$$

for each reaction i. For the Rogers-Chinitz model, the rates are given by[18]

$$k_{f1} = A_1 T^{-10} e^{-4865/R^0 T} \tag{12}$$

$$k_{f2} = A_2 T^{-13} e^{-42{,}500/R^0 T} \tag{13}$$

where

$$A_1 = (8.917\phi + 31.433/\phi - 28.95)(10^{47}) \text{ cm}^3/\text{mol-s}$$

$$A_2 = (2.0 + 1.333/\phi - 0.833\phi)(10^{64}) \text{ cm}^6/\text{mol}^2\text{-s}$$

and

$$K_1 = 26.164 e^{-8992/T}$$

$$K_2 = 2.682 \times 10^{-6} T e^{69415/T}$$

Knowing the reaction rates for Eqs. (12) and (13), one can find the production of the four species present in the model from the law of mass action. For a general reaction,

$$\sum_{j=1}^{N_s} \gamma'_{ij} C_j \underset{k_{bi}}{\overset{k_{fi}}{\rightleftharpoons}} \sum_{j=1}^{N_s} \gamma''_{ij} C_j, \quad i = 1,2,\ldots,N_R$$

the law of mass action states that the rate of change of concentration of species j by reaction j is given by[19]

$$(\dot{C}_j)_i = (\gamma''_{ij} - \gamma'_{ij}) \left(k_{fi} \prod_{j=1}^{N_s} C_j^{\gamma'_{ij}} - k_{bi} \prod_{j=1}^{N_s} C_j^{\gamma''_{ij}} \right) \tag{14}$$

The rate change in concentration of species j by all N_R reactions is then found by summing the contributions from each reaction,

$$\dot{C}_j = \sum_{i=1}^{N_R} (\dot{C}_j)_i \tag{15}$$

Finally, the production rate of species j is found from

$$\dot{w}_j = \dot{C}_j M_j \tag{16}$$

Applying the law of mass action to the global model, Eqs. (8) and (9), give[18]

$$\dot{C}_{O_2} = -k_{f1} C_{H_2} C_{O_2} + k_{b1} C_{OH}^2 \tag{17}$$

$$\dot{C}_{H_2O} = 2(k_{f2} C_{OH}^2 C_{H_2} - k_{b2} C_{H_2O}^2) \tag{18}$$

$$\dot{C}_{H_2} = \dot{C}_{O_2} - \tfrac{1}{2} \dot{C}_{H_2O} \tag{19}$$

$$\dot{C}_{OH} = -(2\dot{C}_{O_2} + \dot{C}_{H_2O}) \tag{20}$$

The source terms for the last i equations in Eq. (2) can now be determined as a function of the dependent variables by application of Eq. (16).

Thermodynamics Model

The specific heat c_p at constant pressure is nearly a linear function of temperature for each species present in the flowfield (H_2, O_2, OH, H_2O, N_2) over the range of temperature being considered. We therefore fit the c_p-vs-temperature data[20] for each species i with

$$c_{p_i}(T) = a_i T + b_i \tag{21}$$

where a and b are constants. (Higher-order fits of specific heat vs temperature could, of course, be used when the dependence was more strongly nonlinear.) A mixture specific heat $\bar{c}_p$ can then be defined by weighting over the species i as

$$\bar{c}_p = \sum_{i=1}^{N_s} c_{p_i} f_i \tag{22}$$

The total enthalpy of the mixture, made up of the five species, is given by

$$H = \sum_{i=1}^{N_s} f_i \left(\int_{T_R}^{T} c_{p_i} dT + H^0_{T_i} \right) + \frac{u^2}{2} \tag{23}$$

where H^0_T is the reference enthalpy at the reference temperature $T_R = 0$ K.[20] Putting Eq. (21) into Eq. (23) and integrating gives

$$H = \sum_{i=1}^{N_s} f_i \left(\frac{a_i T^2}{2} + b_i T + H^0_{T_i} \right) + \frac{u^2}{2} \tag{24}$$

Finally, the mixture gas constant $\bar{R}$ is found by weighting the individual gas constants over the species i as

$$\bar{R} = \sum_{i=1}^{N_s} R_i f_i \tag{25}$$

Equations (22), (24), and (25) can then be used to define all other required thermodynamic variables.

Solution of the Governing Equations

Chebyshev Spectral Method

The Chebyshev spectral collocation method[15] is used to define the derivatives $\partial F/\partial x$ in Eq. (2). This approach yields a spectrally accurate method in space; i.e., the method converges faster in space for a properly resolved case than any power of $1/n$, where n is the number of grid points.[16] To define $\partial F/\partial x$, we expand F in terms of the Chebyshev polynomials,

$$T_n(x) = \cos(n \cos^{-1} x) \tag{26}$$

in the truncated Chebyshev series

$$F(x) = \sum_{n=0}^{N} \hat{F}_n T_n(x) \tag{27}$$

where the $\hat{F}_n$ are the expansion coefficients of the series. To form a range on x, we introduce the change of variables

$$x = \cos\theta, \quad 0 \le \theta \le \pi \tag{28}$$

Putting Eq. (28) into Eq. (26) and introducing the resulting expression into Eq. (27) gives

$$F(x) = \sum_{n=0}^{N} \hat{F}_n \cos n\theta \tag{29}$$

a Fourier cosine series. To discretize Eq. (29), we define a set of collocation points x_j by

$$x_j = \cos(\pi j/N), \quad j = 0,1,2,\ldots,N \tag{30}$$

and the discrete form of Eq. (29) becomes

$$F_j = F(x_j) = \sum_{n=0}^{N} \hat{F}_n \cos\left(\frac{n\pi j}{N}\right) \tag{31}$$

The inverse of Eq. (31) gives the $\hat{F}_n$ as

$$\hat{F}_n = \frac{2}{N\bar{C}_n} \sum_{j=0}^{N} \bar{C}_j^{-1} F_j \cos\left(\frac{n\pi j}{N}\right) \tag{32}$$

where

$$\bar{C}_j = 2, \quad j = 0 \text{ or } j = N$$
$$= 1, \quad 1 \le j \le N-1$$

Examination of Eqs. (31) and (32) shows that the $\hat{F}_n$ can be efficiently evaluated using the fast Fourier transform.[21]

Next, we differentiate F in Eq. (27) with respect to x obtaining

$$F'(x) = \sum_{n=0}^{N} \hat{F}_n T_n'(x) \tag{33}$$

A form of Eq. (33) without derivatives of the Chebyshev polynomials is preferred, so we rewrite Eq. (33) in terms of another series,

$$F'(x) = \sum_{n=0}^{N} \hat{F}_n^{(1)} T_n(x) \tag{34}$$

and then proceed to relate the coefficients of the two series. The following recursion relation exists between the Chebyshev polynomials and their derivatives[15]:

$$\frac{T_{n+1}'}{n+1} - \frac{T_{n-1}'}{n-1} = \frac{2}{C_n} T_n \tag{35}$$

where

$$C_n = 2, \quad n = 0$$
$$= 1, \quad n \ge 1$$

Putting Eq. (35) into Eq. (34) and algebraically manipulating the resulting expression gives

$$F'(x) = \sum_{n=1}^{N} \frac{C_{n-1}\hat{F}_{n-1}^{(1)}}{2n} T_n' - \sum_{n=1}^{N} \frac{\hat{F}_{n+1}^{(1)}}{2n} T_n' \tag{36}$$

Introducing Eq. (33) into Eq. (36) and simplifying then results in

$$2n\hat{F}_n = C_{n-1}\hat{F}_{n-1}^{(1)} - \hat{F}_{n+1}^{(1)} \tag{37}$$

an expression for the $\hat{F}_n^{(1)}$ given the $\hat{F}_n$. The procedure for finding the $\hat{F}_n^{(1)}$ is initialized by setting

$$\hat{F}_{N+1}^{(1)} = 0 \qquad \hat{F}_N^{(1)} = 0$$

and then solving for $\hat{F}_{N-1}^{(1)}$ through $\hat{F}_0^{(1)}$ by back-substitution.[15] Then, with knowledge of all the $\hat{F}_n^{(1)}$, the required spatial derivatives of F can be calculated from Eq. (34). This procedure can again be done efficiently using the fast Fourier transform (FFT).

In summary, the computational procedure to find $\partial F/\partial x$ is carried out as follows. First, given initial values of $F_j = F(x_j)$, find the Chebyshev coefficients $\hat{F}_n$ from Eq. (32) or the FFT. Next, compute the $\hat{F}_n^{(1)}$ from Eq. (37). Then knowing the $\hat{F}_n^{(1)}$, compute $\partial F/\partial x$ from Eq. (34) or the FFT. Once $\partial F/\partial x$ and the source term H [see Eq. (2)] are known at $t = 0$, the solution may be advanced in time with an appropriate temporal integration scheme. The scheme developed for this work is discussed in the next section.

Temporal Integrator

Once values for $\partial F/\partial x$ and H are determined as described previously, there remains a system of ordinary differential equations in time that must be solved for the dependent variable vector U. A number of algorithms were surveyed for integrating this system of ODE's, including pure explicit schemes, pure implicit schemes, and mixed explicit-implicit schemes. The pure explicit schemes were, in general, unattractive because the stiffness of the ODE system made the algorithm inefficient. Pure implicit schemes were also precluded by the difficulty of developing spectral algorithms for the spatial derivatives evaluated implicitly. Hybrid explicit-implicit algorithms therefore appeared to offer the most attractive approach. Following Refs. 4-6, the explicit-implicit split was formed by computing the source term H implicitly at the new time level and computing $\partial F/\partial x$ explicitly at the old time level to allow application of the spectral approach. With this choice, the equations were then integrated in time using a two-stage Runge-Kutta technique, which proved to be effective for use with the Chebyshev spectral method applied in space. The algorithm was developed as follows.

We first discretize Eq. (2) as noted previously, obtaining

$$U_i^{n+1} = U_i^n - \Delta t\left[\left(\frac{\partial F}{\partial x}\right)_{i_{sp}}^{n} + H_i^{n+1}\right] + \mathcal{O}(\Delta t)^2 \tag{38}$$

where n is the old time level and $n+1$ is the new time level. The vector H^{n+1} is then expanded in a Taylor series in time:

$$H^{n+1} = H^n + \Delta t\left(\frac{\partial H}{\partial t}\right)^n + \mathcal{O}(\Delta t)^2$$

or

$$H^{n+1} = H^n + K^n(U^{n+1} - U^n) + \mathcal{O}(\Delta t)^2 \tag{39}$$

where K^n is the Jacobian of H, $\partial H/\partial U$. Putting Eq. (39) into Eq. (38), simplifying the resulting equation, and then rewriting in delta form gives

$$[I + \Delta t K_i^n]\Delta U_i^{n+1} = -\Delta t\left[\left(\frac{\partial F}{\partial x}\right)_{i_{sp}}^{n} + H_i^n\right] \tag{40}$$

where $\Delta U_i^{n+1} = U_i^{n+1} - U_i^n$. Examination of Eq. (40) shows that the bracketed term on the left-hand side is a block-diagonal matrix, the blocks being $n \times n$ submatrices, with n the number of equations in the system of Eq. (2). Since the matrix in Eq. (40) is diagonal, Eq. (40) is the most easily solved for ΔU by inverting the blocks, i.e.,

$$\Delta U_i^{n+1} = -\Delta t[I + \Delta t K_i^n]^{-1} R_i^n \tag{41}$$

where $[\ ]^{-1}$ represents a block invert and

$$R_i^n = \left(\frac{\partial F}{\partial x}\right)_{i_{sp}}^{n} + H_i^n \tag{42}$$

is the steady-state residual vector. The two-stage Runge-Kutta technique, which is second-order accurate in time, is then applied to Eq. (41), yielding the following predictor-corrector formula:

$$\Delta \overline{U_i^{n+1}} = -\Delta t[I+\Delta t K_i^n]^{-1} R_i^n$$

$$U_i^{n+1} = U_i^n + \Delta \overline{U_i^{n+1}} \tag{43}$$

$$\Delta U_i^{n+1} = -\Delta t[I+\Delta t K_i^n]^{-1} \overline{R_i^{n+1}}$$

$$U_i^{n+1} = U_i^n + \tfrac{1}{2}(\Delta \overline{U_i^{n+1}} + \Delta U_i^{n+1}) \tag{44}$$

A formal derivation of the order of accuracy of this method is given in Ref. 22. Starting with initial conditions for U, Eqs. (43) and (44) are used to advance the solution from time level n to time level $n+1$. The process is continued until steady-state conditions, defined as a reduction of 10 orders of magnitude in the steady-state residuals, are reached.

The magnitude of the time step in Eqs. (43) and (44) is chosen based on the physical time scales present at any given time in the solution. The fluid-dynamic time step Δt_f can be shown numerically to be limited by the Courant condition

$$\Delta t_f \leq \Delta x/(|u|+c) \tag{45}$$

The chemical relaxation time for a species i is given by[23]

$$t_c = \rho f_i/\dot{w}_i \tag{46}$$

Changes in this relaxation time are then given by

$$\Delta t_c = \Delta(\rho f_i)/\dot{w}_i \tag{47}$$

since $\dot{w}_i$ remains nearly constant over a time step. For accuracy, we require that the chemical time step be chosen such that no change in specific mass fraction greater than Λ occurs over that time step. Equation (47) then becomes

$$\Delta t_c = \Lambda/\dot{w}_i \tag{48}$$

where Λ is initially set at 0.0001 for the computations that follow. The computational time step Δt is then chosen to be the minimum over all grid points of the fluid and chemical time step, i.e.,

$$\Delta t = \min(\Delta t_f, \Delta t_c) \tag{49}$$

Initial and Boundary Conditions

The governing equations [Eqs. (2)] are hyperbolic and require initial conditions at each point to start the calculation and boundary conditions at the inflow boundary. Initial conditions are computed by first specifying an inflow Mach number and estimating an outflow Mach number. The interior Mach number distribution is then assumed to have a spatial variation which is linear. The total pressure and total temperature are assumed to be constant throughout the domain. Finally, the initial flow is assumed to be isentropic, so that isentropic relations can be used to compute the static pressure and temperature; these conditions are found from

$$T_0/T = 1 + [(\gamma-1)/2]M^2 \tag{50}$$

$$p_0/p = (T_0/T)^{\gamma/(\gamma-1)} \tag{51}$$

Knowing the static temperature and pressure and Mach number, we can compute the velocity distribution, and the density distribution can be found from the equation of state. Since the inflow boundary flow remains supersonic, boundary conditions are specified there by holding conditions fixed at their initial values.

Results

Having now developed a numerical algorithm for solving the equations governing chemically reacting flows, that algorithm will now be used to model the reacting flow in a rapid expansion supersonic diffuser. A rapid expansion diffuser was chosen such that high concentration gradients existed near the inflow boundary, providing a formidable test for the method. Results from the present algorithm were compared with a benchmark calculation from an existing finite-difference chemical kinetics code to validate the method. The comparison also allowed a demonstration of performance of the high-order accurate spectral method on grids which were quite coarse compared to grids required in the finite-difference calculation.

The rapid expansion diffuser is shown in Fig. 1. The diffuser is 2 units long and has an initial cross-sectional area of 0.79 and a final cross-sectional area of 3.14. The diffuser wall is defined, as noted, by a shifted sinusoidal. Flow is introduced to the diffuser at $M=1.4$, a velocity of 1230 m/s, a temperature of 1900 K, and a pressure of 0.081 MPa. The chemical composition of the inflow is defined to be a 3/10 stoichiometric mixture of hydrogen fuel and air.

Starting from the initial state described above, the governing equations were solved, using the algorithm in a time consistent manner, until steady-state conditions were reached. Independent benchmark calculations were also carried out with a previously validated Adams-Moulton implicit finite-difference program. In the results which follow, comparisons between the two methods will be made, first to verify the new procedure and second to demonstrate its high spatial resolution on relatively coarse grids. A comparison of

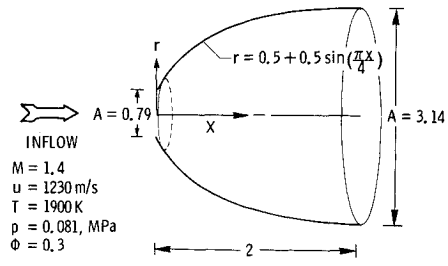

Fig. 1 Rapid expansion supersonic diffuser test case.

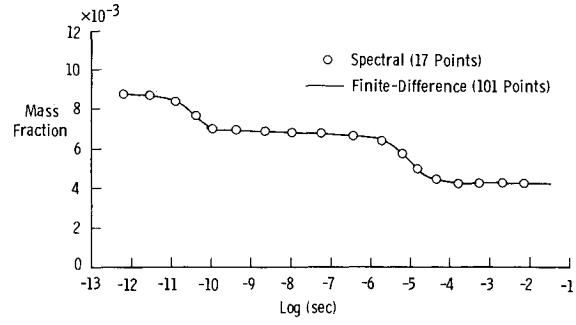

Fig. 2 Comparison of the time history of hydrogen mass fraction.

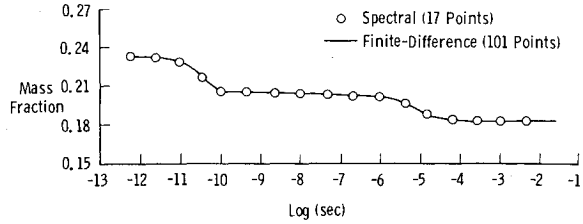

Fig. 3 Comparison of the time history of oxygen mass fraction.

methods showing a time history of the chemical species is given in Figs. 2-4 for H_2, O_2, OH, and H_2O, respectively. Results are presented at the first grid point interior to the inflow boundary, where both the flowfield and species gradients are a maximum. Agreement between the Runge-Kutta spectral and finite-difference calculations is excellent in all cases.

Next we compare spatial results from the two methods once steady-state conditions have been reached. The finite-difference solution required 101 grid points on a uniform grid before a grid independent solution, defined as a graphically imperceptible difference in the steady-state result between the present grid and next coarser grid, was attained. Calculations using the Runge-Kutta spectral code were carried out on 17- and 9-point Chebyshev grids. Comparisons of steady-state results for the two methods are given in Figs. 5-10. Figure 5 shows a comparison of the axial velocity profiles in the diffuser. The 17-point spectral solution and the finite-difference solutions agree quite well throughout the diffuser; the 9-point spectral solution slightly overpredicts the velocity near the inflow boundary but agrees well throughout the remainder of the diffuser. The overprediction is likely due to the failure of the coarsest spectral grid to predict adequately the high gradients that exist at the beginning of the diffuser. Temperature comparisons, given in Fig. 6, follow similar trends, with the 17-point spectral solution agreeing well with the benchmark, and the 9-point solution also agreeing well, except near the inflow boundary. Identical trends also occur when axial pressure profiles are compared in Fig. 7.

Comparisons of axial species distribution computed by the two methods are given in Figs. 8-10. Prediction of the H_2 mass fraction by the spectal method with 17 grid points agrees well with the finite-difference solution throughout the diffuser, as can be seen by examining Fig. 8. The 9-point spectral solution underpredicts the H_2 mass fraction near the inflow boundary, again owing to the high spatial gradient in f_{H_2} there, but agreement again becomes good away from the inflow boundary. The spatial distribution of the O_2 mass fraction is given in Fig. 9. The gradients are not as large for this species, since O_2 is in excess, and both 17- and 9-point grids agree well with the finite-difference solution. The steady-state species distributions for OH and H_2O are given in Fig. 10. The spatial gradients are again high for both species near the inflow boundary, and trends similar to those for H_2 are repeated here. Agreement is again quite good when comparing the 17-point spectral and finite-difference results; however, the 9-point spectral solution still underpredicts gradients near the inflow boundary.

A final comparison of methods is given in Fig. 11 which shows the rate of reduction of steady-state residual with iteration count at the first interior grid point. Since the 17-point Runge-Kutta spectral and the 101-point finite-difference calculations yield comparable accuracy and have the same minimum spatial step size, it is reasonable to assess the relative efficiency of the methods using the result given in Fig. 11. Note that the residual reduction rate by the spectral code is significantly greater than that provided by the finite-difference code. The maximum residual (at any grid point) is reduced with the spectral code by 10 orders of magnitude in only 2400 iterations, whereas the finite-

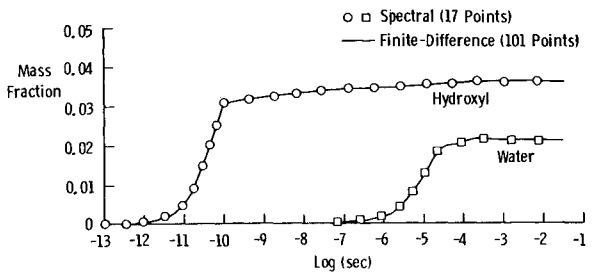

Fig. 4 Comparison of the time histories of the hydroxyl and water mass fractions.

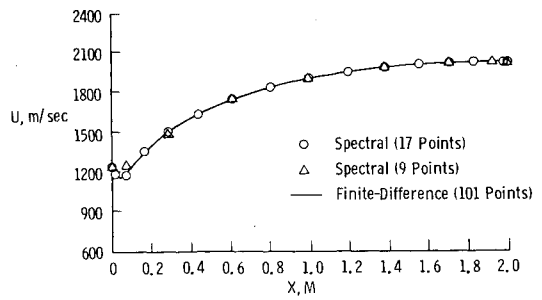

Fig. 5 Comparison of axial velocity profiles.

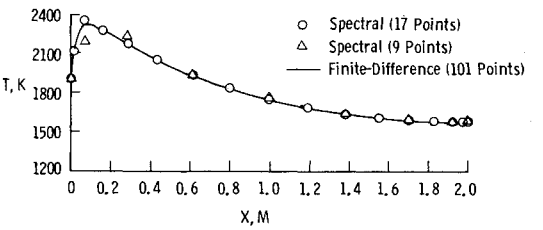

Fig. 6 Comparison of axial temperature profiles.

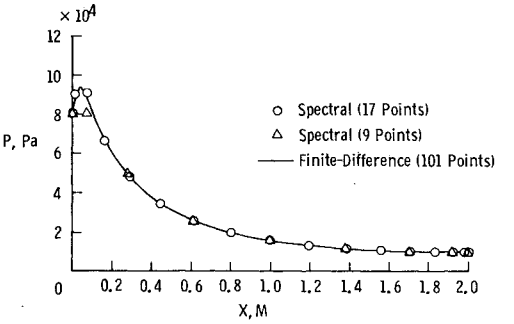

Fig. 7 Comparison of axial pressure profiles.

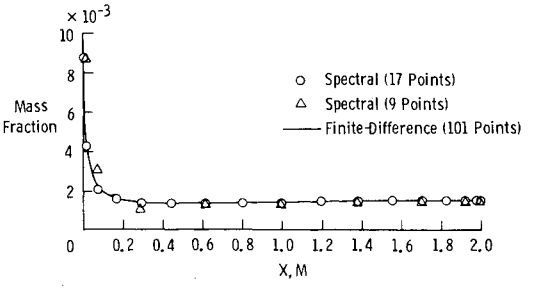

Fig. 8 Comparison of axial hydrogen mass fraction profiles.

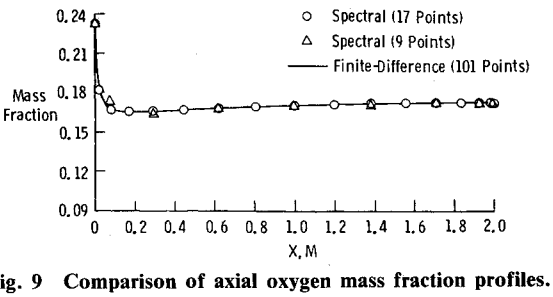

Fig. 9 Comparison of axial oxygen mass fraction profiles.

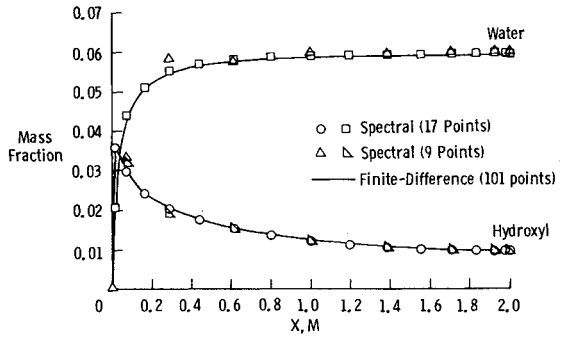

Fig. 10 Comparison of axial hydroxyl and water mass fraction profiles.

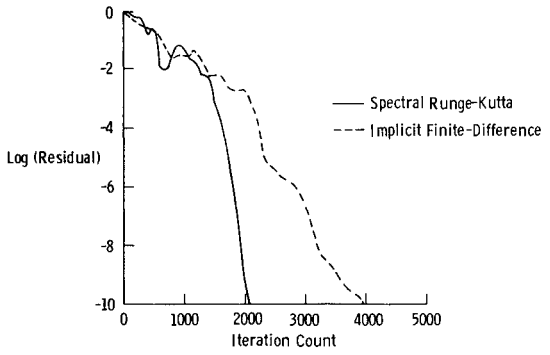

Fig. 11 Comparison of the steady-state residual reduction rates of the methods.

difference code requires 6000 iterations to achieve the same level of residual reduction. The more rapid rate of residual reduction along with the coarse grid translates directly into an overall computational efficiency of the spectral Runge-Kutta method. The spectral program requires 105 s on a CYBER-175 computer to reach steady-state conditions, whereas the finite-difference program requires 2524 s to reach steady state on the same machine. Following this comparison, we attempted to improve the performance of the finite-difference code by applying several other temporal integrators and by solving on Chebyshev grids up to 129 points. It was found, however, that no calculations performed as well as the orginal Adams-Moulton method on the 101-point uniform grid, and, in fact, most computations performed much worse.

Concluding Remarks

A numerical method has been developed for solving the equations governing chemically reacting flowfields. In this method, spatial derivatives are discretized using a Chebyshev spectral collocation technique. Species source terms are calculated using a global hydrogen-air finite-rate chemistry model. The resulting ordinary differential equations in time are integrated using a two-stage, partial implicit Runge-Kutta scheme that is effective in handling the stiffness due to chemical kinetics, that is present in these equations. A computer program has been used to compute the flow in a rapid expansion supersonic diffuser. The diffuser flowfield was also computed using an existing implicit finite-difference reacting flow code that had been validated in prior analyses. A comparison of results from the two programs indicated that the Runge-Kutta spectral code was accurate in predicting both the time evolution of the dependent variables and the final steady-state results. In addition, the spectral algorithm produced equivalent accuracy on relatively coarse grids as compared to the fine grid required by the finite-difference calculations. Based on these results, it appears that the Runge-Kutta spectral method offers promise for improving our ability to model chemically reacting flowfields.

References

[1]Drummond, J. P. and Weidner, E. H., "Numerical Study of a Scramjet Engine Flow Field," *AIAA Journal*, Vol. 20, Sept. 1982, pp. 1182-1187.

[2]Drummond, J. P., Rogers, R. C., and Evans, J. S., "Combustion Modeling for Scramjet Engines," AGARD Conference Proceedings No. 275, Oct. 1979, pp. 10.1-10.30.

[3]Drummond, J. P., "Numerical Study of a Ramjet Dump Combustor Flow Field," *AIAA Journal*, Vol. 23, April 1985, pp. 604-611.

[4]Bussing, T.R.A. and Murman, E. M., "A Finite Volume Method for Calculation of Compressed Chemically Reacting Flows," AIAA Paper 85-0331, Jan. 1985.

[5]Stalnaker, J. F., Robinson, M. A., Spradley, L. W., Kurzius, S. C., and Thoenes, J., "Development of the General Interpolants Method for the Cyber 200 Series of Computers," Report TR D867354, Lockheed-Huntsville Research and Engineering Center, Huntsville, AL, Oct. 1983.

[6]Smoot, L. D., Hecker, W. C., and Williams, G. A., "Prediction of Propagating Methane-Air Flames," *Combustion and Flame*, Vol. 26, June 1976, pp. 323-342.

[7]Gear, G. W., *Numerical Initial Value Problems in Ordinary Differential Equations*, Prentice Hall, Englewood Cliffs, NJ, 1971.

[8]Hindmarsh, A. C., "GEAR: Ordinary Differential Equation Solver," Rept. UCID-30001, Lawrence Livermore Laboratory, Livermore, CA, 1974.

[9]Hindmarsh, A. C. and Byrne, G. D., "EPISODE: An Effective Package for the Integration of Systems of Ordinary Differential Equations," Rept. UCID-30112, Lawrence Livermore Laboratory, Livermore, CA, 1977.

[10]Liniger, W. and Willoughby, R. A., "Efficient Integration Methods for Stiff Systems of Ordinary Differential Equations," *SIAM Journal of Numerical Analysis*, Vol. 7, March 1970, pp. 47-66.

[11]Pratt, D. T., "Exponential-Fitted Methods for Integrating Stiff Systems of Ordinary Differential Equations," CPIA Pub. 401, 1984 JANNAF Propulsion Meeting, Feb. 1984, pp. 53-67.

[12]Bui, T.D., Oppenheim, A. K., and Pratt, D. T., "Recent Advances in Methods for Numerical Solution of O.D.E. Initial Value Problems," Rept. LBL-16943, Lawrence Berkeley Laboratory, University of California, Berkeley, CA, 1983.

[13]Radhakrishnan, K., "Comparison of Numerical Techniques for Integration of Stiff Ordinary Differential Equations Arising in Combustion Chemistry," NASA TP-2372, Oct. 1984.

[14]Hussaini, M. Y., Kopriva, D. A., Salas, M. D., and Zang, T. A., "Spectral Methods for the Euler Equations," *AIAA Journal*, Vol. 23, Feb. 1985, pp. 234-240.

[15]Hussaini, M. Y., Salas, M. D., and Zang, T. A., *Spectral Methods for Inviscid, Compressible Flows. Advances in Computational Transonics*, edited by W. G. Habashi, Pineridge Press, Swansea, 1983.

[16]Gottlieb, D. and Orszag, S. A, "Numerical Analysis of Spectral Methods, Theory and Applications," CBMS-NSF, Regional Conference Series in Applied Mathematics, SIAM, 1977.

[17]Dwyer, H. A. and Sanders, B. R., "Modeling of Unsteady Combustion Phenomena," AIAA Paper 77-136, Jan. 1977.

[18]Rogers, R. C. and Chinitz, W., "Using a Global Hydrogen-Air Combustion Model in Turbulent Reacting Flow Calculations," *AIAA Journal*, Vol. 21, April 1983, pp. 586-592.

[19]Williams, F. A., *Combustion Theory*, Addison-Wesley, Reading, MA, 1965.

[20]McBride, B. J., Heimel, S., Ehlens, J. G., and Gordon, S. "Thermodynamic Properties to 6000°K for 210 Substances Involving the First 18 Elements," NASA SP-3001, 1963.

[21]Brigham, E. O., *The Fast Fourier Transform*, Prentice Hall, Englewood Cliffs, NJ, 1974.

[22]Beckett, R. and Hurt, J., *Numerical Calculations and Algorithms*, McCraw-Hill, New York, 1967, pp. 202-210.

[23]Li, C. P., "Time Dependent Solutions of Nonequilibrium Air Flow Past a Blunt Body," AIAA Paper 71-595, June 1971.